Numerical simulation of turbulent flow through a straight square duct using a near wall linear $k-\varepsilon$ model.

Ahmed Rechia[1], Hassan Naji[2,*], Gilmar Mompean[2], and Abdelatif El Marjani[3]

[1]Faculté des Sciences et Technologies de Tanger,
B.P 416 Tanger, Maroc
ahmed.rechia@polytech-lille.fr

[2]Université des Sciences et Technologies de Lille, Polytech-Lille,
LML - UMR CNRS 8107, Boulevard P. Langevin,
59655 Villeneuve d' Ascq, France
hassan.naji@polytech-lille.fr
gilmar.mompean@polytech-lille.fr

[3]Ecole Mohammadia d'Ingénieurs, Laboratoire de TurboMachines
Avenue Ibn Sina B.P 765 - Agdal, Rabat, Maroc
marjani@emi.ac.ma

ABSTRACT

The aim of this work is to predict numerically the turbulent flow through a straight square duct using Reynolds Average Navier-Stokes equations (RANS) by the widely used $k-\varepsilon$ and a near wall turbulence $k-\varepsilon-f_\mu$ models. To handle wall proximity and no-equilibrium effects, the first model is modified by incorporating damping functions f_μ via the eddy viscosity relation. The predicted results for the streamwise, spanwise velocities and the Reynolds stress components are compared to those given by the $k-\varepsilon$ model and by the direct numerical simulation (DNS) data of Gavrilakis (J. Fluid Mech., 1992). In light of these results, the proposed $k-\varepsilon-f_\mu$ model is found to be generally satisfactory for predicting the considered flow.

Key words: Computational fluid mechanics; Reynolds Average Navier-Stokes k-epsilon turbulence models; finite-volume CFD algorithm; duct flow.

1. INTRODUCTION

The prediction of turbulent flows involving secondary motions and using numerical simulations of the Reynolds Average Navier-Stokes (RANS) equations has great practical value in fluid mechanics and many applications can be found in centrifugal machinery design. In these simulations, the aim is to obtain accurate values of pressure and velocity for the flow field. Among the various RANS models for turbulence, the two-equation turbulence $k-\varepsilon$ models have found their broad applications of feasibility in the majority of engineering practice for the predictions of the complex turbulent flows. By far the most popular turbulence model is the standard $k-\varepsilon$ model which is

*Author to whom all correspondence should be addressed.

based on the linear stress-strain relation initially proposed by Boussinesq. This type of closure has been revealed robust and efficient with respect to CPU time than more high-order models [1,2].

In this work, the numerical investigation of a low Reynolds number turbulent flow through a straight square duct is carried out in order to describe its turbulent characteristics. In spite of appearances, this flow is difficult to carry out numerically and/or experimentally. This configuration has been frequently chosen by many authors [3,4,5,6,7] since it is a relatively simple geometry which provides a good case test to improve turbulence models. Note that this flow is anisotropic and involves a secondary flow in the cross-stream plane, which is absent in the case of a plane channel. This secondary flow convects mean flow momentum from the centre of the duct to the corners. This causes a bulging of the streamwise velocity contours towards the corners. By studying the origin of the secondary flow for the square duct, Mompean [8] and Huser et al. [9], using DNS data of this problem, concluded that the streamwise vorticity is responsible for the generation of the secondary flow. The equation of mean vorticity in the streamwise direction, $\Omega = \partial\overline{W}/\partial y - \partial\overline{V}/\partial z$, reads as:

$$\overline{V}\frac{\partial\Omega}{\partial y} + \overline{W}\frac{\partial\Omega}{\partial z} = \frac{\partial}{\partial y\partial z}\left(\overline{v^2} - \overline{w^2}\right) + \left(\frac{\partial^2}{\partial z^2} - \frac{\partial^2}{\partial y^2}\right)\overline{vw} + \nu\nabla^2\Omega \qquad (1)$$

where $\overline{V}$ *and* $\overline{W}$ are the mean spanwise and normal velocities, $\overline{v^2}$ and $\overline{w^2}$ are the turbulent normal stresses, $\overline{vw}$ is the cross-stream correlation and v is the Kinematic viscosity.

From this formulation, the three terms on the right side of the above equation can be interpreted as the vorticity production (which is linked to the anisotropy of the cross-stream normal stresses), the production term due to the cross-stream correlation $\overline{vw}$ and the vorticity viscous dissipation. As the Reynolds number of the flow increases, the viscous dissipation term tends to be negligible and other terms become relevant. According to these authors, it seems therefore possible that the streamwise vorticity has its origin in the inequality of the normal Reynolds stresses combined with a presence of lateral wall gradient. In other words, the vorticity production term, $\partial(\overline{v^2} - \overline{w^2})/\partial y\partial z$, plays a crucial role in the generation of secondary flows.

It is well known that traditional two-equation models are incapable of describing such flows. While, traditional two-equation models, the standard $k-\varepsilon$ model, fail to predict the near wall behaviour and anisotropy of the normal Reynolds stresses, it is shown in this paper that these standard $k-\varepsilon$ eddy viscosity models can be improved via the introduction of damping functions of Van Driest type to produce the anisotropy. Previous studies have been carried out and provided interesting results, see Gavrilakis [10], Huser & Biringen [11] and Xu and Pollard [4] for a low Reynolds number turbulent flow. In this work, the predicted results are compared with the DNS data of Gavrilakis [10], the LES prediction of Xu [4] and the experimental data of Nishino [7] at a Reynolds number 4800 based on the duct hydraulic diameter and on the bulk velocity. As the turbulent characteristics are in good agreement with the DNS and experiment, this provides the motivation for the study of this flow from further models as non-equilibrium models [12] and nonlinear turbulence models [13,14].

The paper is organised as follows: the turbulence model $k-\varepsilon$ and the introduction of damping functions are briefly reported within section 2; the finite volume numerical method is presented in section 3. In section 4, the main results of this work are presented, discussed and finally some conclusions are drawn.

2. GOVERNING EQUATIONS

To predict the turbulent flow, the statistical approach is used applying the Reynolds decomposition, which consists in splitting velocity and pressure into an average and a fluctuating part. As in all studies of Reynolds stress modelling, any flow variable ϕ can be decomposed as follows:

$$\phi = \overline{\phi} + \varphi \tag{2}$$

where $\overline{\phi}$ is the mean turbulent value and φ is the fluctuating component.

The equations governing the mean velocity $\overline{U}_i$ and the mean pressure $\overline{P}$ are obtained from the RANS equations for an incompressible flow:

$$\frac{\partial \overline{U}_i}{\partial x_i} = 0 \tag{3}$$

$$\frac{\partial \overline{U}_i}{\partial t} + \frac{\partial}{\partial x_j}(\overline{U}_i\ \overline{U}_j) = -\frac{1}{\rho}\frac{\partial \overline{P}}{\partial x_j} + \frac{\partial}{\partial x_j}(\nu \frac{\partial \overline{U}_i}{\partial x_j} - \overline{u_i\, u_j}) \tag{4}$$

where ρ is the fluid density and $\tau_{ij} = \overline{u_i\, u_j}$ is the Reynolds stress tensor.

In order to achieve closure of this system of equations, a Reynolds stress model that lies τ_{ij} to the global history of the mean velocity field must be supplemented. A variety of expressions have all independently established that, to the lowest order, τ_{ij} can be represented by the standard eddy viscosity form [15,16]:

$$\tau_{ij} = \frac{2}{3}k\delta_{ij} - \nu_t\, 2\overline{S}_{ij} \tag{5}$$

where k is the turbulent kinetic energy, ν_t is the eddy viscosity, $\overline{S}_{ij} = (\partial \overline{U}_i / \partial x_j + \partial \overline{U}_j / \partial x_i)/2$ is the mean strain rate tensor and δ_{ij} is the Kronecker tensor.

Note that in this approach, the problem was reduced from deriving equations describing the evolution of τ_{ij} to deriving equations for k with an appropriate eddy viscosity ν_t. In this study, the eddy viscosity is expressed as:

$$\nu_t = C_\mu \frac{k^2}{\varepsilon} \tag{6}$$

where ε is the dissipation rate of the turbulent kinetic energy k and C_μ is a model constant.

In the two-equation $k - \varepsilon$ context, the turbulent kinetic energy transport equation is derived from the contraction of the Reynolds stress transport equation, and is given by:

$$\frac{\partial k}{\partial t} + \overline{U}_j \frac{\partial k}{\partial x_j} = \mathbb{D}_k + \mathbb{P}_k - \varepsilon \tag{7}$$

where the right-hand side represents the transport of k by the combined effects of turbulent transport and viscous diffusion $\mathbb{D}_k = \frac{\partial}{\partial x_j}\left(\frac{\nu_t}{\sigma_k}\frac{\partial k}{\partial x_j}\right)$, the turbulent production $\mathbb{P}_k = \nu_t 2\overline{S}_{ij}\frac{\partial \overline{U}_i}{\partial x_j}$ and the isotropic turbulent dissipation ε.

As for the transport equation of the dissipation rate ε, a rather general expression from which many of the forms can be derived. The modelling of this equation is based on analogies with the k equation and on phenomenological considerations. In its most commonly used form, this equation can be written as [17]:

$$\frac{\partial \varepsilon}{\partial t}+\bar{U}_k \frac{\partial \varepsilon}{\partial x_j}=\frac{\partial}{\partial x_j}\left[\frac{\nu_t}{\sigma_\varepsilon}\frac{\partial \varepsilon}{\partial x_j}\right]+C_{\varepsilon 1}\frac{\varepsilon}{k}\ \mathbb{P}_k-C_{\varepsilon 2}\frac{\varepsilon^2}{k} \tag{8}$$

The Eqns. (7)-(8) contain five constants C_μ, $C_{\varepsilon 1}$, $C_{\varepsilon 2}$, σ_k and σ_ε whose values are usually obtained from calibrations with homogeneous shear flows and from the decay rate of homogeneous and isotropic turbulence. The most commonly used values of these constants are:

$$C_\mu = 0.09\,;\ C_{\varepsilon 1} = 1.44;\ C_{\varepsilon 2} = 1.92\,;\ \sigma_k = 1.0\,;\ \sigma_\varepsilon = 1.3\,.$$

This $k-\varepsilon$ model is most commonly used in turbulent shear flow computations with a great deal of success. In the two-equation $k-\varepsilon$ models, Eqns. (7) and (8) in their high-Reynolds number form, do not provide the correct asymptotic behaviour in the wall region. In order to handle near wall effects, damping functions f_μ are associated with the eddy viscosity definition (see for example [18,19]):

$$\nu_t = C_\mu f_\mu \frac{k^2}{\varepsilon} \tag{9}$$

$$\text{with}\quad f_\mu = (1-a\exp(-bz^+))(1-a\exp(-by^+)) \tag{10}$$

where the constants 'a' and 'b' can take various values for each element of the Reynolds stress tensor τ_{ij}. Previous works have been done using a priori test and interesting results have been obtained, see references [20] and [21]. It is this assumption that we adopted in this paper. These corrections allow to incorporate viscous molecular diffusion in the vicinity of solid boundaries. The variables y^+ and z^+ are the wall co-ordinates based on the friction velocity $u_\tau = \sqrt{\frac{\tau_w}{\rho}}$ and the cinematic viscosity ν, $y^+ = u_\tau y/\nu$ and $z^+ = u_\tau z/\nu$.

3. NUMERICAL METHOD

The method used to solve the set of equations (3)-(4)-(7)-(8) is the classical finite volume method (FVM). The conservation equations are integrated over a control volume, and the Gauss theorem is used to transform the volume integrals into surface integrals.

3.1. SPACE DISCRETIZATION

To describe the numerical algorithm, the RANS equations can be written in the form:

$$\frac{\partial \phi}{\partial t}+\frac{\partial}{\partial x_j}(\bar{U}_j\phi)+\frac{\partial}{\partial x_j}(J_\varphi) = S_\varphi \tag{11}$$

where ϕ can be any of the above variables $\left(\bar{U},\bar{V},\bar{W},\bar{P},k,\varepsilon\right)$ and the overbar represents the ensemble average. This is the so-called transport equation for property ϕ. It clearly highlights

Table 1

Equation	Φ	J_ϕ	S_ϕ
Masse conservation	1	0	0
Momentum Eqn.			
x-axis	$\bar{U}$	$\overline{P}\delta_{1j} - \nu\partial\overline{U} / \partial x_j + \left(\overline{uu}\right)_j$	0
y-axis	$\bar{V}$	$\overline{P}\delta_{2j} - \nu\partial\overline{V} / \partial x_j + \left(\overline{vu}\right)_j$	0
z-axis	$\bar{W}$	$\overline{P}\delta_{3j} - \nu\partial\overline{W} / \partial x_j + \left(\overline{wu}\right)_j$	0
Turbulent kinetic energy	k	$-\frac{\nu_t}{\sigma_k}\frac{\partial k}{\partial x_j}$	$-\overline{u_i u_j}\partial\overline{U}_i / \partial x_j - \varepsilon$
Dissipation	ε	$-\frac{\nu_t}{\sigma_\varepsilon}\frac{\partial \varepsilon}{\partial x_j}$	$-C_{\varepsilon 1}\frac{\varepsilon}{k}\overline{u_i u_j}\frac{\partial\overline{U}_i}{\partial x_j} - C_{\varepsilon 2}\frac{\varepsilon^2}{k}$

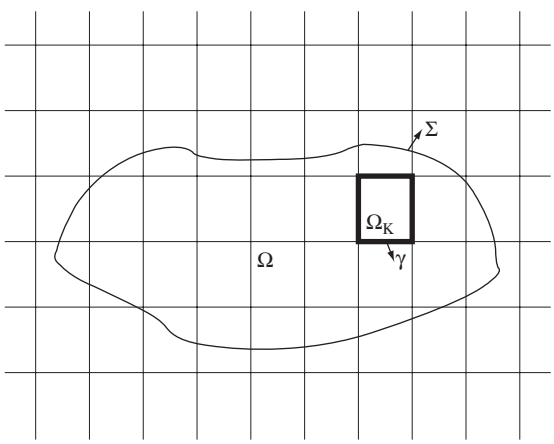

Figure 1 Calculation Domain Ω and control volume Ω_K

the various transport processes. For a Cartesian system (x, y, z), the expressions of the various terms of the equation (11) can be given by (see Table 1). The key step of the finite volume method is the integration of the transport equation (11) over a control volume Ω_k of boundary γ(see Figure 1). Then, applying the Gauss divergence theorem, the resulting equation can be written as follows:

$$\frac{\partial}{\partial t}\int_{\Omega_k}\phi d\Omega + \int_\gamma J_\varphi \vec{U}.\vec{n}d\gamma + \int_\gamma J_\varphi n d\gamma = \int_{\Omega_k} S_\varphi \tag{12}$$

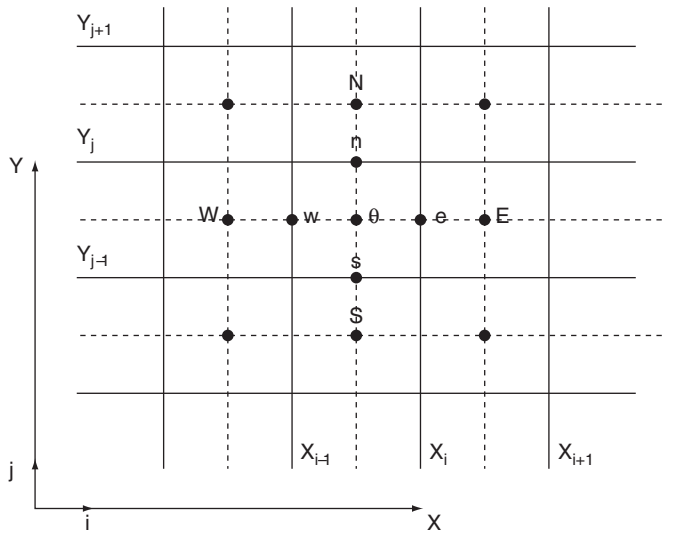

Figure 2 Arrangement for a staggered grid.

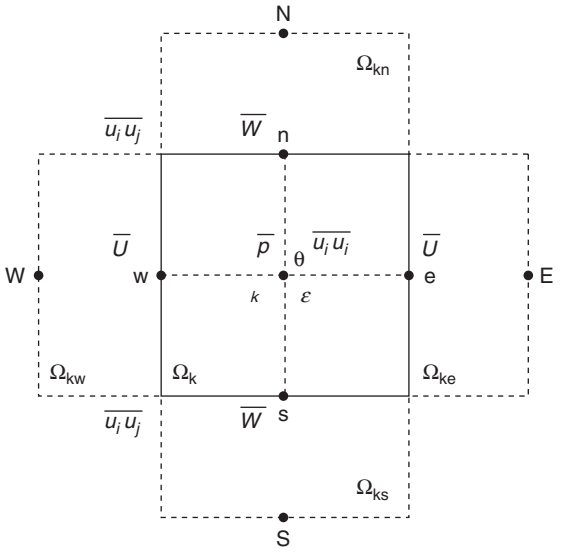

Figure 3 Control volume for a staggered and notation used.

The equation (12) gives the assessment of any scalar flow property ϕ in the control volume Ω_k. This equation is the base of the space discretization of FVM. There is no need for all variables to share the same grid; a staggered mesh may turn out to be advantageous. This arrangement is shown in Figures 2 and 3. To solve the differential equation, a finite volume

numerical method has been employed. The pressure, the turbulent kinetic energy, k, the dissipation, ε, and the normal Reynolds stress components are treated in the center of the control volumes; the velocities are computed in the center of the faces and the cross components of the Reynolds tensor are attached to nodes located at the mid-edges. The biggest advantage of the staggered arrangement is the strong coupling between the velocities and pressure. This helps the avoid some types of the convergence problems and oscillations in pressure and velocity fields.

The integrals volume of the temporal and source term of the equation (12) are approximated by adopting an Eulerian scheme and using the theorem of the average. The advection terms for the momentum equation arising from the finite volume integration are approximated by the quadratic upstream interpolation scheme for the convective kinetics (QUICK) scheme of Leonard [21]. This scheme is second order accurate in space. More details about the numerical procedure are given in [22,23].

3.2. TEMPORAL DISCRETIZATION

The stationary solution was obtained by a time-marching algorithm. For a first order time scheme, the system (3)-(4)-(7)-(8) is written as:

$$\frac{\partial \bar{U}_i^{n+1}}{\partial x_i} = 0 \tag{13}$$

$$\frac{\bar{U}_i^{n+1} - \bar{U}_i^{n}}{\Delta t} + \frac{\partial}{\partial x_j}(\overline{U}_i \overline{U}_j)^n = -\frac{1}{\rho}\frac{\partial \overline{P}_i^{n+1}}{\partial x_j} + \left[\frac{\partial}{\partial x_j}\left(\nu \frac{\partial \overline{U}_i}{\partial x_j} - \overline{u_i u_j}\right)\right]^n \tag{14}$$

$$\frac{K_i^{n+1} - K_i^{n}}{\Delta t} = -\bar{U}_j^n \frac{\partial K_i^n}{\partial x_j} + \nu_t \frac{\partial \bar{U}_i^n}{\partial x_j} 2S_{ij}^n - \varepsilon_i^n + \frac{\partial}{\partial x_j}\left[\frac{\nu_t}{\sigma_k}\frac{\partial K_i^n}{\partial x_j}\right] \tag{15}$$

$$\frac{\varepsilon_i^{n+1} - \varepsilon_i^{n}}{\Delta t} = -\bar{U}_i^n \frac{\partial \varepsilon_i^n}{\partial x_j} + C_{\varepsilon 1}\nu_t \frac{\varepsilon_i^n}{K_i^n}\frac{\partial \bar{U}_i^n}{\partial x_j} 2S_{ij}^n - C_{\varepsilon 2}\frac{\varepsilon_i^{n2}}{K_i^n} + \frac{\partial}{\partial x_j}\left[\frac{\nu_t}{\sigma_\varepsilon}\frac{\partial \varepsilon_i^n}{\partial x_j}\right] \tag{16}$$

where the superscript n is the previous time step and $n + 1$ is the next one.

The convective, diffusive, production and dissipation terms of the different transport equations are treated by an explicit Euler scheme. The advection terms in the $k - \varepsilon$ equation are discretized in space using the first order upwind scheme. The diffusion terms are discretized with a second-order cell-centred scheme. The pressure is treated by an implicit scheme, where the decoupling procedure for the pressure is derived from the Marker and Cell (MAC) algorithm proposed by Harlow and Welch [24]. The method of solution consists in substituting the equation for the velocity at the new time n + 1 within the discretized equation for mass conservation at the same time level. With this method, the pressure at the next time step n+1 is obtained by the resolution of the discretized Poisson equation. Then, the velocities are calculated from the momentum equations. Since the linear system for the pressure equation is symmetric and positive definite, it can be solved by the Cholesky procedure or by a preconditioned conjugate method. Note that the principle of mass flux continuity is imposed indirectly via the solution of this equation. Convergence was declared when the maximum normalized sum of absolute residual $\tilde{\varepsilon}^n$ for each variable ϕ over all the

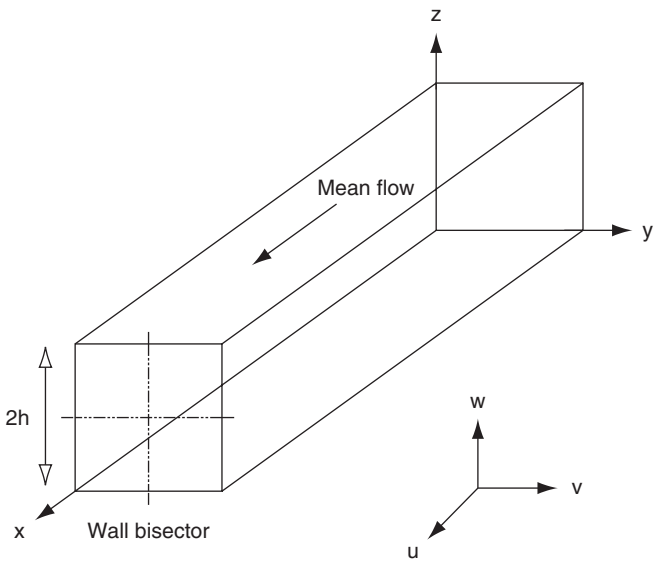

Figure 4 Flow geometry and axes system.

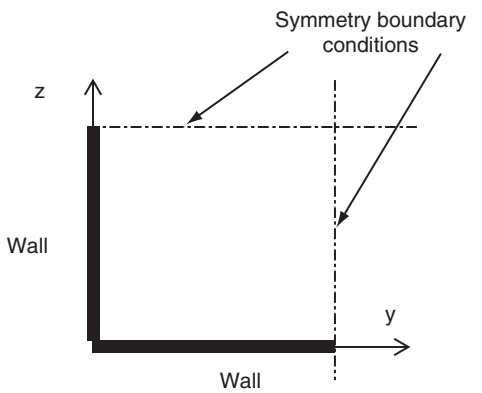

Figure 5 Quadrant of the square.

computational domain was less than 10^{-4}. This maximum error is for each variable determined as:

$$\tilde{\varepsilon}^n = Max\left(\sum_{i=1}^{N}\frac{(\phi_i^{n+1}-\phi_i^{n})}{\phi_i^{n+1}}\right)$$

where N is the number of control volumes.

3.3 COMPUTATIONAL DOMAIN AND BOUNDARY CONDITIONS

The geometrical configuration the square duct with the reference axes is shown in figure 4. The x-axis designates the streamwise direction. The normal direction is parallel to the y-axis and the spanwise direction is parallel to the z-axis. The cross-section is divided into four quadrants. Because of symmetry, only quadrant of the square need to be calculated with symmetry conditions at the center (see figure 5).

For the first time-step, at the inlet of the duct, a constant profile was given to $\bar{U}$, k and ε. The secondary velocities were initialised as nil ($\bar{V} = 0$ and $\bar{W} = 0$) all over the domain. The k and ε inlet values were obtained from the DNS data using the r.m.s velocities ($u_{rms} = (\tau_{ii}/3)^{1/2}$) and the eddy viscosity, that was about four times the molecular viscosity. At the outlet, a homogeneous Neumann boundary condition was used for all variables. In the next time-step, the calculated outlet values were used for the inlet condition. The same procedure is used for the following time-steps up to the convergence.

The calculations were carried out using 41×41 grid points, regularly spaced in the cross-section and five grid points in the streamwise direction. The outcome with this grid was found to be satisfactory. The grid convergence was checked using 21×21 grid points in the cross-section, the maximum difference observed between the two calculations were less than 1% in the streamwise velocity near the corner ($z/h = 0.1$). A test case with 20 grid points in the streamwise direction and 21×21 in the cross-section was made in order to check the grid independence in the streamwise direction, and no relevant difference was observed because the maximum difference was about 2% for the spanwise velocity at $z/h = 0.16$.

The boundary condition values for k and ε, at the first grid point near the wall, was calculated taking into account the fact that this point was in the viscous sub-layer (always $y^+ \prec 5$). Also, due to the use of a staggered grid, the value of k and ε are not defined at the wall. In this paper, we consider the following boundary conditions for the equation of k and ε, which have been used by Patel et al. [19]:

$$\frac{\partial k}{\partial y} = 0 \text{ or } \quad \frac{\partial k}{\partial z} = 0, \text{ and } \quad \varepsilon = \nu \frac{\partial^2 k}{\partial y^2} \quad \text{or} \quad \varepsilon = \nu \frac{\partial^2 k}{\partial z^2}$$

When this is done, it is necessary to modify the model itself near the wall. It is argued that the effects that need to be modelled are due to the low Reynolds number near the wall and a number of low Reynolds number modifications of the $k - \varepsilon$ model have been proposed; see Patel et al. [19] and Wilcox [25] for a review of these modifications.

A condition for symmetry, homogeneous Neumann, was used for all the variables along the wall bisectors of the square duct.

4. RESULTS

This section shows the results for a turbulent flow in a square duct quadrant using the linear $k - \varepsilon$ model with and without damping functions f_μ. Direct Numerical Simulation (DNS) of Gavrilakis [10] is used to compare some turbulence characteristics.

The developed turbulent flow through a straight square duct has been simulated. The DNS has been carried out for the Reynolds number based on the hydraulic diameter of the duct (2h) and the mean flow velocity $\bar{U}_m$ is 4800. The Reynolds number based on the friction velocity u_τ, is $\mathrm{Re}_\tau = u_\tau 2h/\nu = 320$. The velocity ratio $\bar{U}_0/\bar{U}_m$ for this configuration was 1.33, $\bar{U}_0$ being the mean centreline velocity. The maximum Kolmogorov scale is $1.5\nu/u_\tau$. In the following, the presentation of the characteristics of the flow are confined to one duct quadrant.

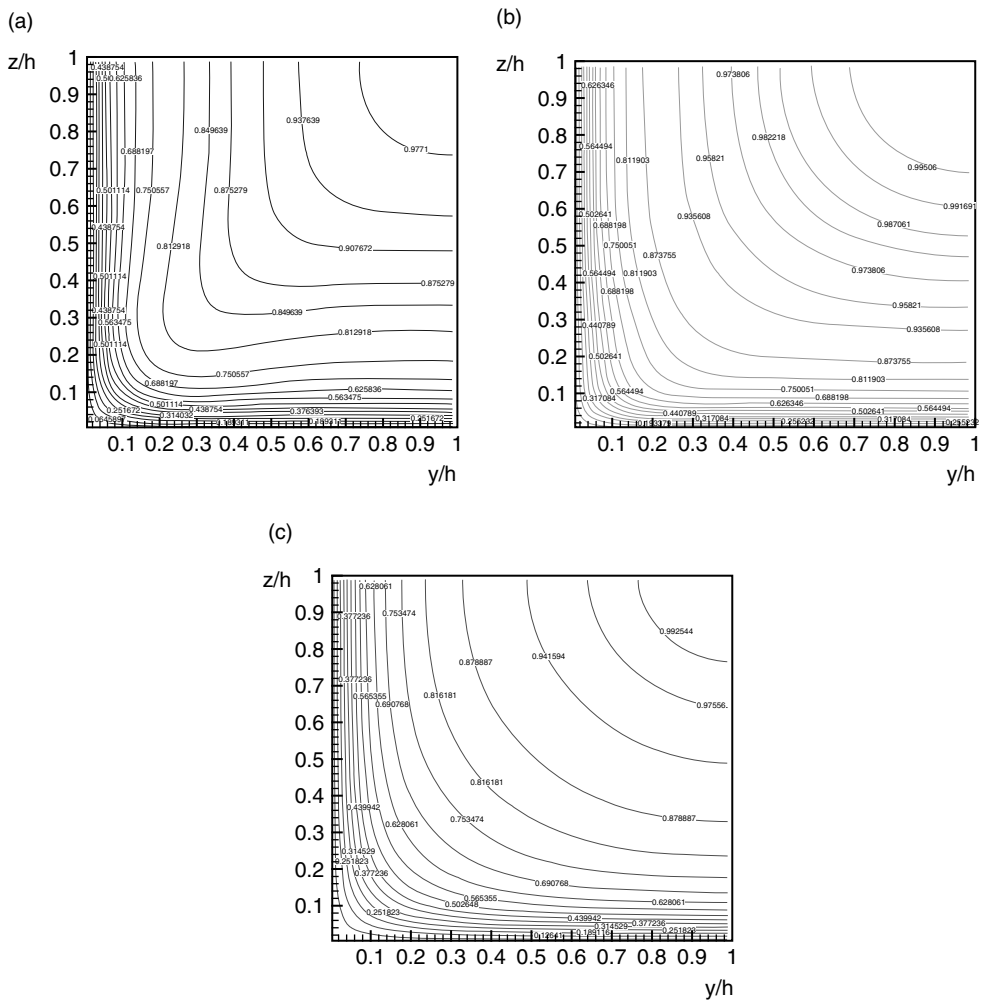

Figure 6 Streamwise flow contours obtained from (a) DNS, (b) $k-\varepsilon-f_{\mu}$, (c) $k-\varepsilon$.

Figure 6 shows the contours of streamwise velocity for one quadrant, obtained with the standard $k-\varepsilon$ model**,** the $k-\varepsilon-f\mu$ model and the DNS. By the examination of this figure, we remark that the flow is symmetric according the corner bisector. The predictions are in good agreement with DNS data. The model $k-\varepsilon$ is unable to predict the effect of vortex induced by the secondary flow on the contours.

The profiles of the mean streamwise velocity ($\overline{U}$) for several section are shown in Figure 7(a)-(c) respectively, for $y/h = 0.1$, 0.5 and 1.0. In these figures, we show the comparisons between the linear $k-\varepsilon$ model, the $k-\varepsilon-f\mu$ model, DNS of Gavrilakis [10] and the experimental data of Cheesewright et al. [27]. At the section $y/h = 0.1$, Figure 7(a) shows a strong distortion on the mean velocity generated by the secondary flow. On the other hand, the linear $k-\varepsilon$ model used was unable to predict this distortion on the mean streamwise velocity

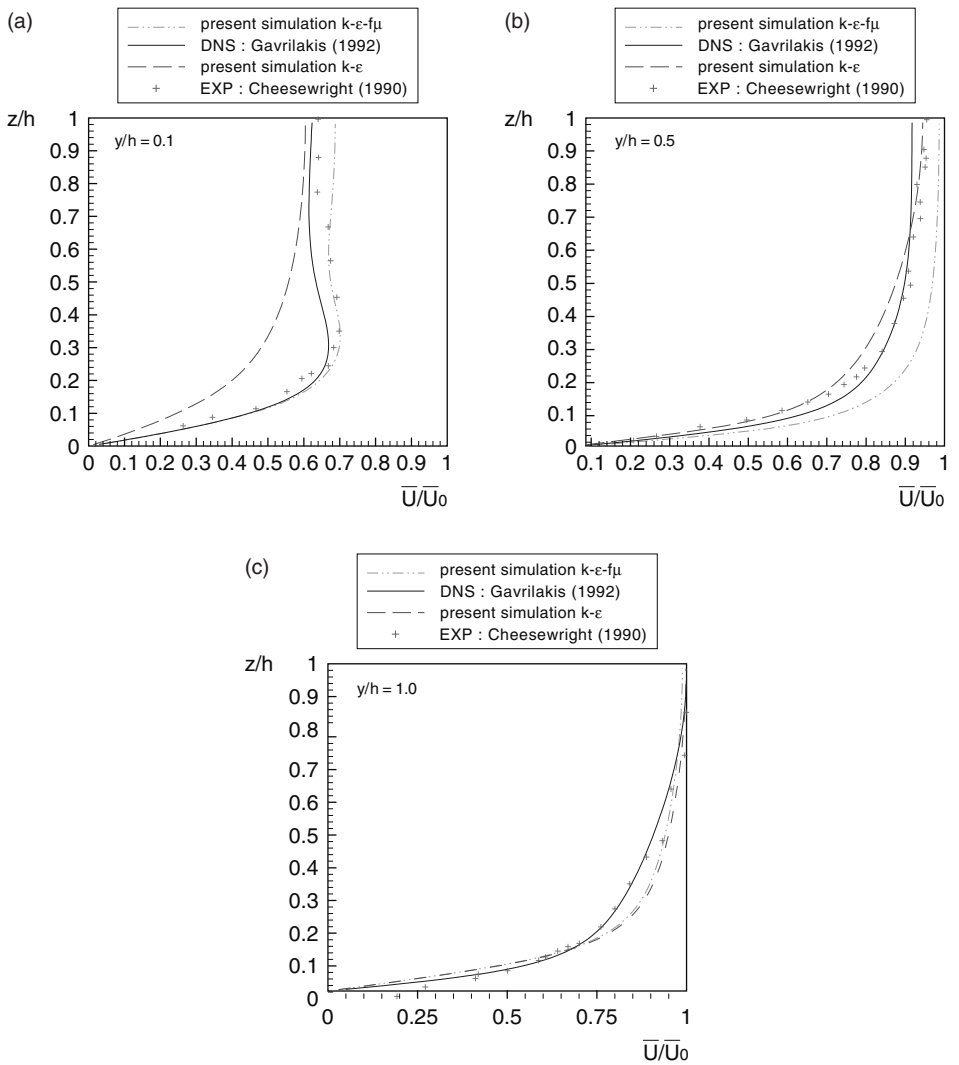

Figure 7 The dimensionless mean streamwise velocity profiles at different sections: (a) y/h = 0.1, (b) y/h = 0.5, (c) y/h = 1.

in this region. After $y/h = 0.5$, the agreement between the results of the different models and experiments starts to improve, and is good at the wall bisector (see Figure 7c, $y/h = 1.0$).

The comparisons between the two models, DNS of Gavrilakis and experimental data [26] for the spanwise velocity $\left(\overline{V}\right)$ are presented in figure 8(a) and 8(b), respectively, for two sections, $z/h = 0.1$ and $z/h = 0.8$.

There is a good qualitative agreement between the various datasets of DNS, measurements and $k-\varepsilon-f\mu$. At $z/h = 0.8$, we note that the spanwise velocity $\left(\overline{V}\right)$ is overall well predicted by

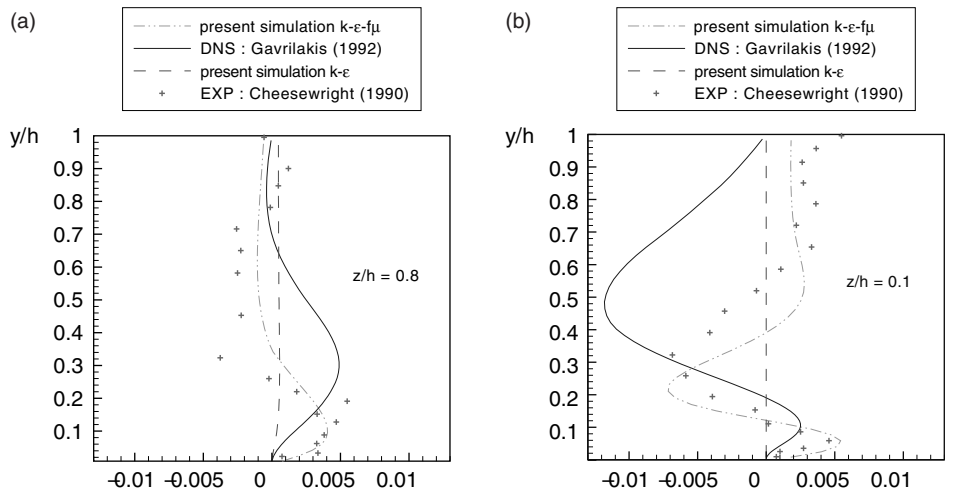

Figure 8 The dimensionless mean spanwise velocity profiles along two sections: (a) $z/h = 0.1$, (b) $z/h = 0.8$.

Table 2 Values of constants 'a' and 'b' used in the f_μ function

	$\overline{uu}^+$	$\overline{vv}^+$	$\overline{ww}^+$	$-\overline{uw}^+$
a	–4.16	1.	0.5	–0.5
b	0.06	0.05	0.001	0.047

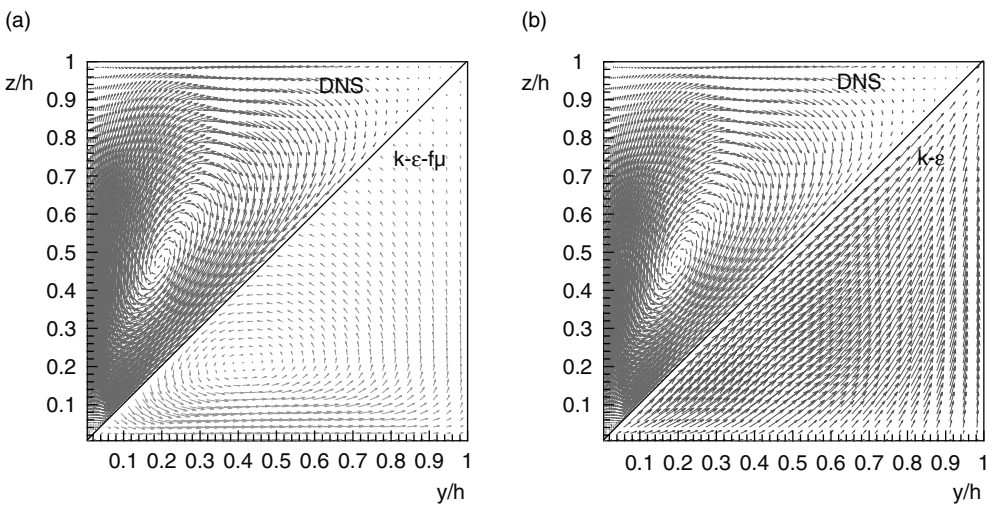

Figure 9 Secondary velocity vectors. (a) DNS square duct (left side) and $k-\varepsilon-f\mu$ model results (right side); (b) DNS square duct (left side) and $k-\varepsilon$ model results (right side).

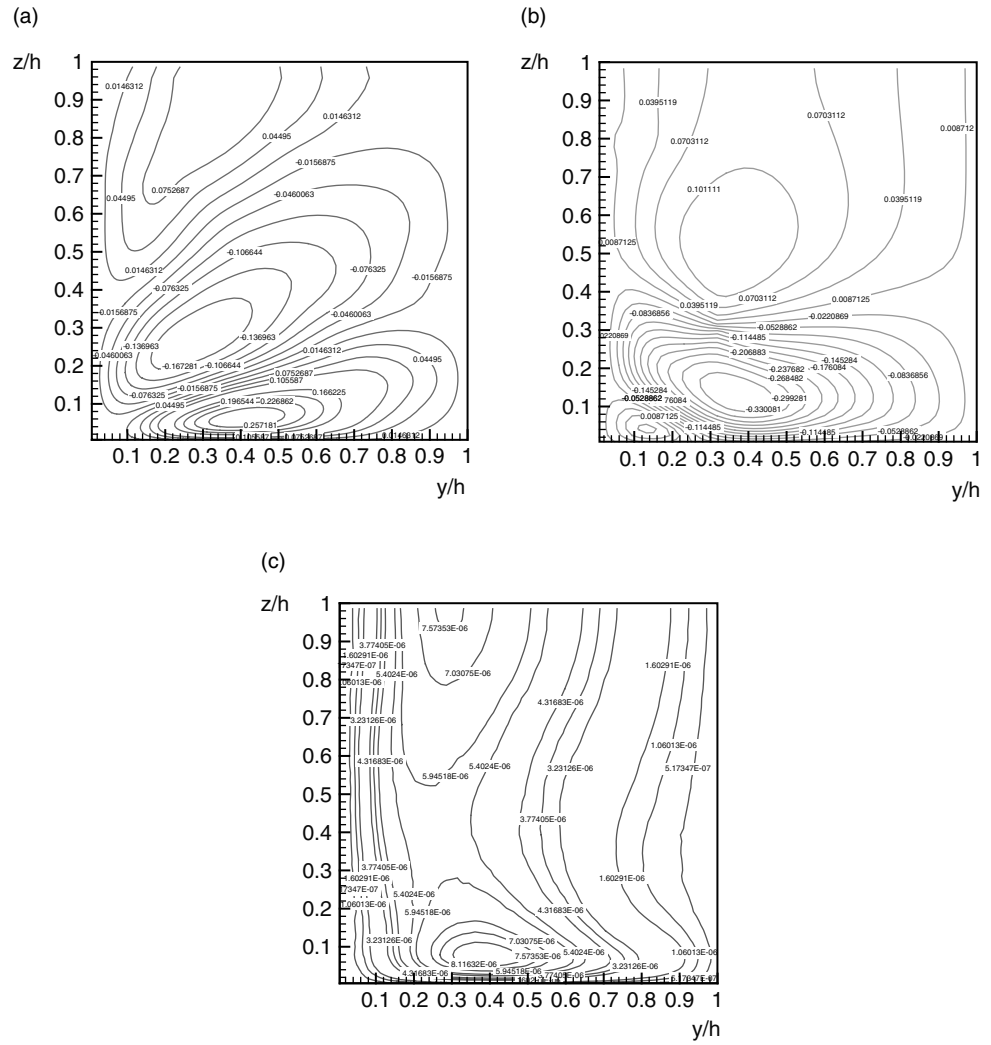

Figure 10 The dimensionless spanwise flow contours obtained with the (a) DNS, (b) $k-\varepsilon-f\mu$, (c) $k-\varepsilon$.

the $k-\varepsilon-f\mu$ model, but the level of $(\bar{V})$ is underpredicted at the position of strong velocity, e.g. at $y/h \approx 0.2$ (see Figure 8(a)). It is also noted that the difference between the $k-\varepsilon-f\mu$ model and the DNS data, in the region of strong velocity, decreases as z/h increases. The linear $k-\varepsilon$ does not give any secondary flow ($\bar{V}=0$) for all the values of z/h.

The figure 9 depicts the secondary velocity vectors in the quadrant obtained from DNS, $k-\varepsilon-f\mu$ and $k-\varepsilon$ models. The DNS results are shown on the left side of the diagonal, and the $k-\varepsilon-f\mu$ or the $k-\varepsilon$ results model on the right side (cf. Figure 9(a) and 9(b) respectively). As can be seen, the $k-\varepsilon-f\mu$ model is able to capture reasonably the vortices

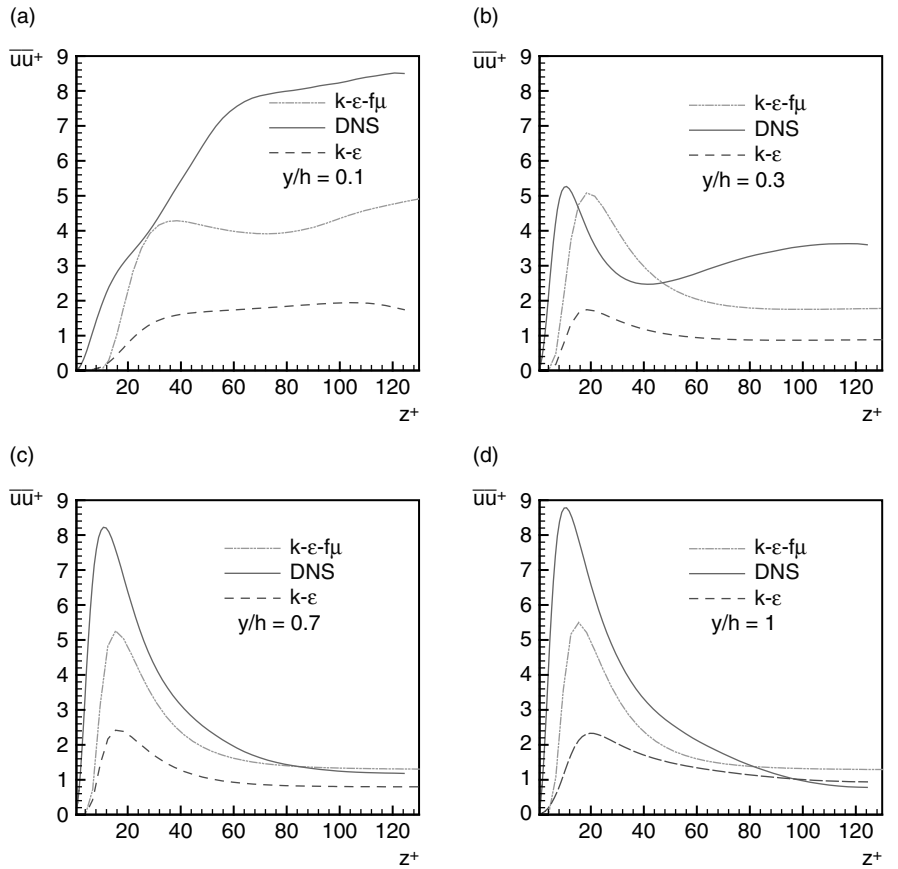

Figure 11 The normal Reynolds stress $\overline{uu}^+$ profiles along the wall bisector at y/h = 0.1, 0.3, 0.7 and 1.0. Comparison of the predictions of the $k-\varepsilon$ and $k-\varepsilon-f\mu$ models with DNS.

structure. In other words, it is apparent that the cross-flow plane contains a vortex along the y and z – walls and the secondary vector field seems to be similar to that obtained by Gavrilakis [26].

In Figure 10(c), we can observed clearly that the spanwise contours obtained by the $k-\varepsilon$ model are not satisfactory. On the other hand, the spanwise contours obtained by the $k-\varepsilon-f\mu$ model are compared favourably with those of the DNS data (see Figures 10(a) and 10(b)).

In order to well predict the profiles of the Reynolds stresses, we have introduced the damping functions $f\mu$ (see Eqn. (10)) whose the main role is to describe better the pattern of the flow in the near-wall regions. According to our simulations, the best values of constants 'a' and 'b' which allow the reproduction of the Reynolds stresses $\overline{u_i u_i}^+ = \overline{u_i u_i}/u_\tau^2, \left(1 \le i \le 3\right)$ and $-\overline{uw}^+ = -\overline{uw}/u_\tau^2$ are given in Table 2.

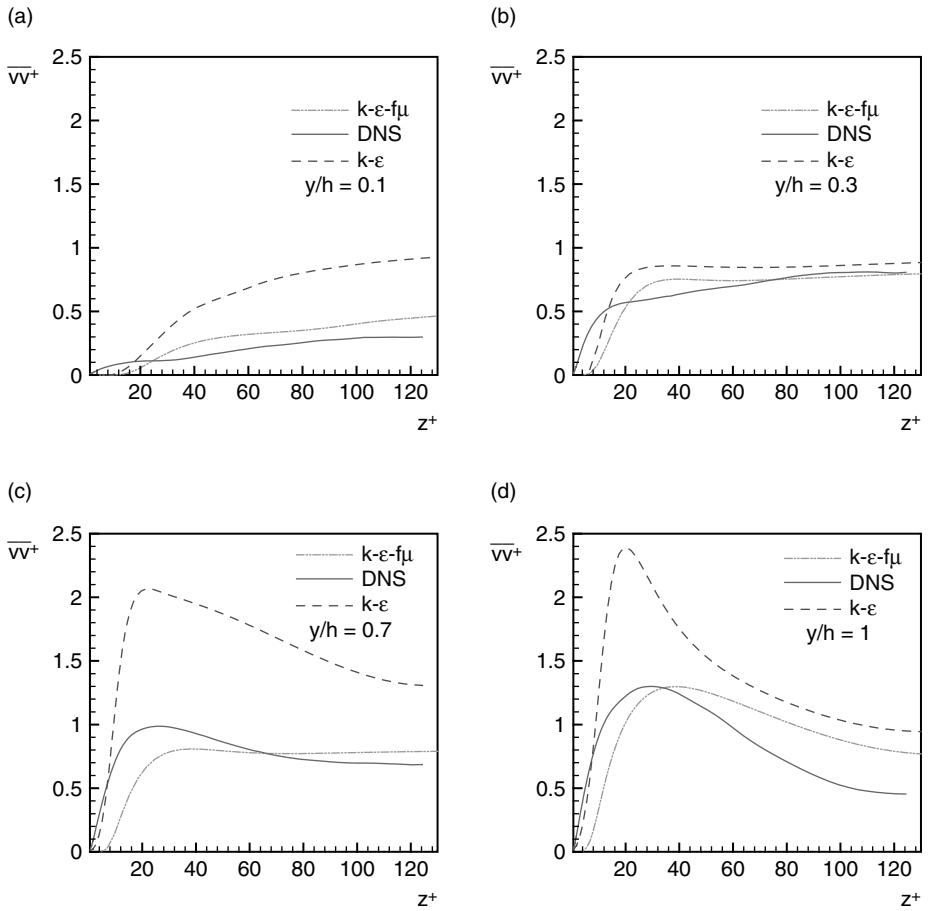

Figure 12 The normal Reynolds stress $\overline{vv}^+$ along the wall bisector at y/h = 0.1, 0.3, 0.7 and 1.0. Comparison of the predictions of the $k-\varepsilon$ and $k-\varepsilon-f\mu$ models with DNS.

In Figures 11, 12, 13 and 14, comparisons between the two models and direct numerical simulation data for the three normal Reynolds stresses $\overline{uu}^+$, $\overline{vv}^+$, $\overline{ww}^+$ in four different sections (y/h = 0.1, 0.3, 0.7 and 1.0) and for the shear stress $-\overline{uw}^+$ in two sections (y/h = 0.7, 1.0) along the wall bisector are shown.

The distribution of the primary normal stress $\overline{uu}^+$ along the wall bisector for sections y/h = 0.1, 0.3, 0.7 and 1.0 predicted by the $k-\varepsilon$ and the $k-\varepsilon-f\mu$ models are presented in Figure 11. We note that the $k-\varepsilon-f\mu$ model gives a better overall agreement with the DNS data at y/h = 0.7 and y/h = 1.0. This quantity is rather well predicted in the region $z^+ \succ 50$ starting from the section y/h = 0.7. We clearly see that the maximum of this quantity given by the $k-\varepsilon-f\mu$ is highly improved. The linear $k-\varepsilon$ underpredicts this component in all the sections. At the section y/h = 1.0, the maximum of the normal stress $\overline{uu}^+$ is underestimated

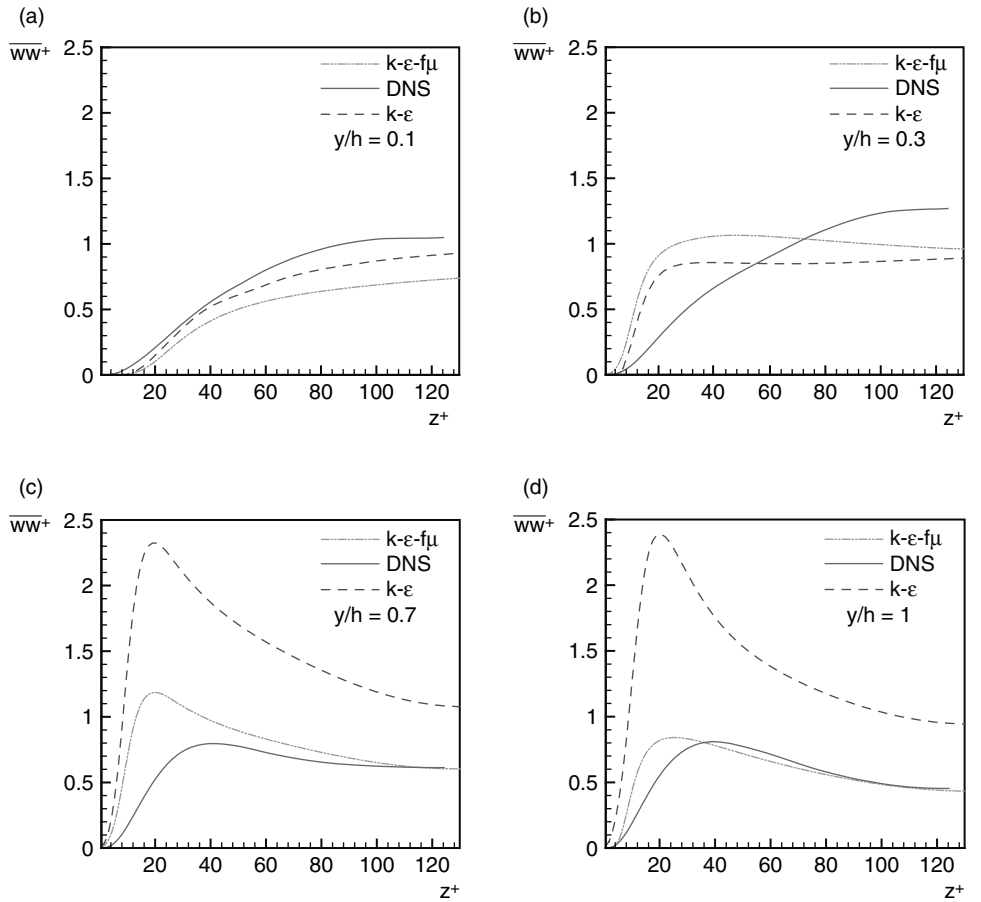

Figure 13 The normal Reynolds stress $\overline{ww}^+$ along the wall bisector at $y/h = 0.1$, 0.3, 0.7 and 1.0. Comparison of the predictions of the $k-\varepsilon$ and $k-\varepsilon-f\mu$ models with DNS.

by about 70% by the $k-\varepsilon$ model. However, when the $k-\varepsilon-f\mu$ model is used, this difference can be reduced up to 35% (cf. Figure 11d).

The profiles of the normal Reynolds stress components $\overline{vv}^+$ and $\overline{ww}^+$ and the tangential stress $-\overline{uw}^+$ along the wall bisector given by the $k-\varepsilon$ and $k-\varepsilon-f\mu$ models are shown in Figures 12, 13 and 14 respectively. It seems clear that the $k-\varepsilon$ model cannot correctly reproduce all these stresses whereas the $k-\varepsilon-f\mu$ model gives very good results in particular for $y/h = 0.7$ and $y/h = 1.0$. When considering the secondary normal stress $\overline{vv}^+$ (cf. Figure 12), the results from the $k-\varepsilon-f\mu$ model are in overall agreement with the DNS at $y/h = 0.1$, 0.3, 0.7, whereas at $y/h = 1.0$, some substantial differences remain in particular for $z^+ \succ 50$ (cf. Figure 12d). As for the $k-\varepsilon$ model, it overpredicts this quantity for $z^+ \succ 10$ starting from the section $y/h = 0.1$. Considering the normal stress $\overline{ww}^+$ (see Figure 13), the $k-\varepsilon-f\mu$ model agrees well with the DNS, especially in the region $z^+ \geq 40$ at $y/h = 0.7$ and $y/h = 1.0$. However, at $y/h = 0.3$ (see Figure 13b), the two models give completely different

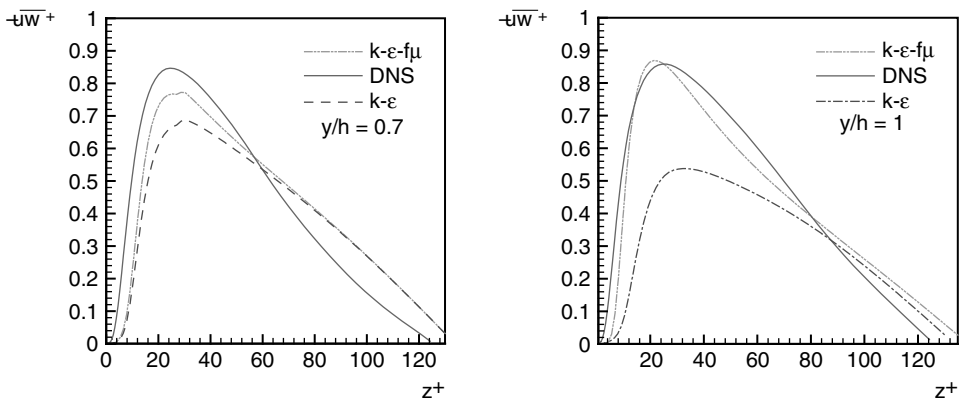

Figure 14 The dimensionless Reynolds stress $-\overline{uw}^{+}$ along the wall bisector at y/h = 0.7 and 1.0. Comparison with DNS.

results from those given by the DNS. At $y/h = 0.7$ and $y/h = 1.0$, the $k-\varepsilon$ model overpredicts highly the results.

Figure 14 shows the profile of the primary shear stress $-\overline{uw}^{+}$ obtained by the $k-\varepsilon$ and $k-\varepsilon-f\mu$ models. At $y/h = 0.7$ and $y/h = 1.0$, the differences among results of the $k-\varepsilon-f\mu$ models are not substantial. The results of $y/h = 0.7$ from the $k-\varepsilon$ model, indicate that this model underpredicts slightly this component for $0 \prec z^{+} \prec 60$, whereas at $y/h = 1.0$, they indicate that the model underpredicts even more this quantity for $0 \prec z^{+} \prec 90$. It is also noted that the $k-\varepsilon-f\mu$ model predicts the right position of the peak of the primary shear stress $-\overline{uw}^{+}$ at $z^{+} \approx 25$ (cf. Figure 14).

Figure 15 displays the normal Reynolds stresses $\overline{uu}^{+}$, $\overline{vv}^{+}$, $\overline{ww}^{+}$ and the primary shear stress $-\overline{uw}^{+}$ profiles along the wall bisector of the square duct at centreline ($y/h = 1.0$). These values are compared with the DNS of Gavrilakis [10], the LES of Xu and Pollard [4] and the experimental data from Nishino and Kasagi [7]. In global sense, the predicted results by the $k-\varepsilon-f\mu$ model disclose that this model can gives an overall agreement. It is seen that the discrepancy is rather weak the secondary normal stresses $\overline{vv}^{+}$, $\overline{ww}^{+}$ and for the shear stress $-\overline{uw}^{+}$ indicating that our methodology may be considered as sufficient.

The distribution of the turbulent kinetic energy from the DNS and the $k-\varepsilon-f\mu$ model are compared in Figure 16. The differences among our results and the DNS are not substantial. The $k-\varepsilon-f\mu$ model yields better results than the results of the $k-\varepsilon$ model (see Fig. 16c). The figure 16b shows the results of the $k-\varepsilon-f\mu$ model indicating a qualitatively good agreement of k with the profile obtained by DNS.

5. CONCLUSION

The purpose of this paper is to describe a study of the turbulent flow in a straight square duct which involves a secondary flow. The spatial discretization of the RANS equations is performed by a finite volume method with a staggered variable arrangement.

The linear $k-\varepsilon$ model is employed for the prediction of the considered flow. This model has been modified by using different damping functions. The present corrections were validated

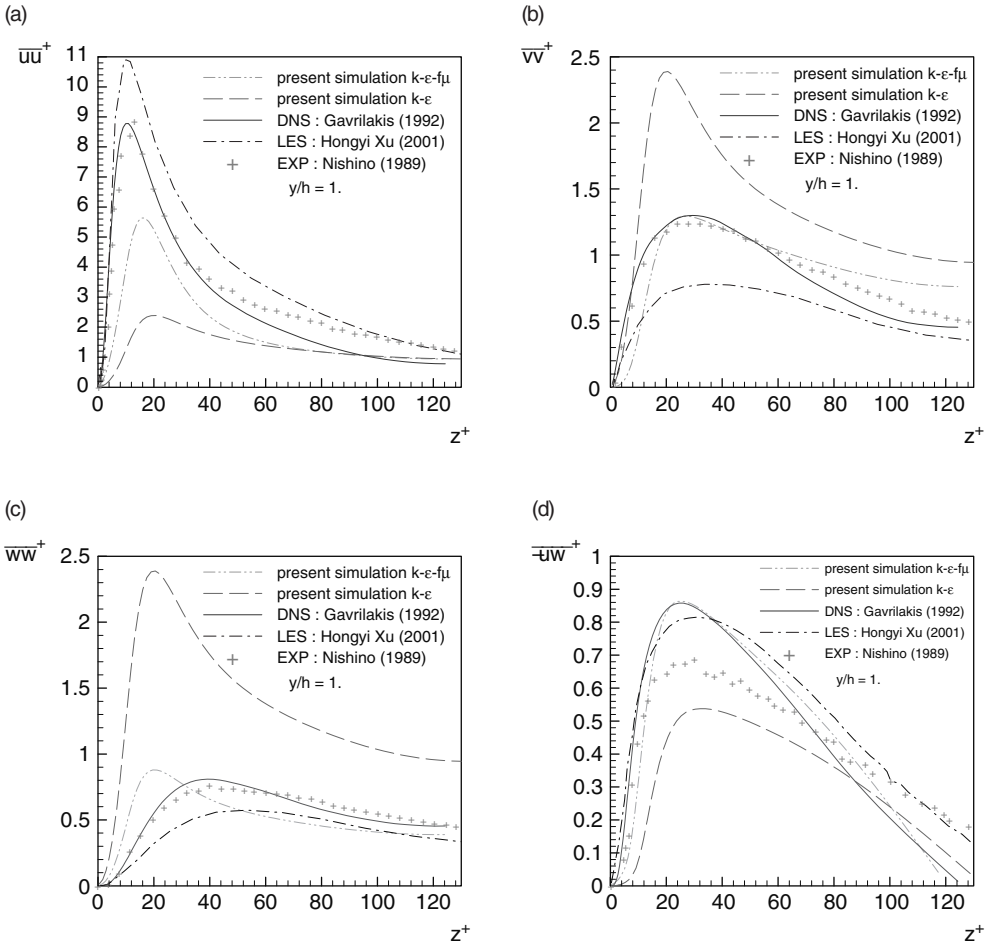

Figure 15 The dimensionless Reynolds stresses $\overline{u_i u_i}^+, \left(1 \le i \le 3\right)$ and $-\overline{uw}^+$ along the wall bisector at $y/h = 1.0$. Comparison of the predictions of the $k-\varepsilon$ and $k-\varepsilon-f\mu$ models with DNS, LES and experiment.

by comparing the calculated velocity profiles and the turbulent quantities with the available direct numerical simulation data given in Ref. [10]. These comparisons yielded the following conclusions:

- Mean velocity profiles are, in general, in good agreement with the DNS data in particular when one approaches the center of the duct ($y/h = 1.0$ or $z/h = 1.0$).
- Although some discrepancies exist for the turbulent quantities, the $k-\varepsilon-f\mu$ model leads to similar results.
- The evaluation of the considered model with DNS data reveals that some anisotropy close to the wall can be captured.
- The $k-\varepsilon-f\mu$ model tested in this work yields considerably better predictions than those obtained by the standard $k-\varepsilon$ model.

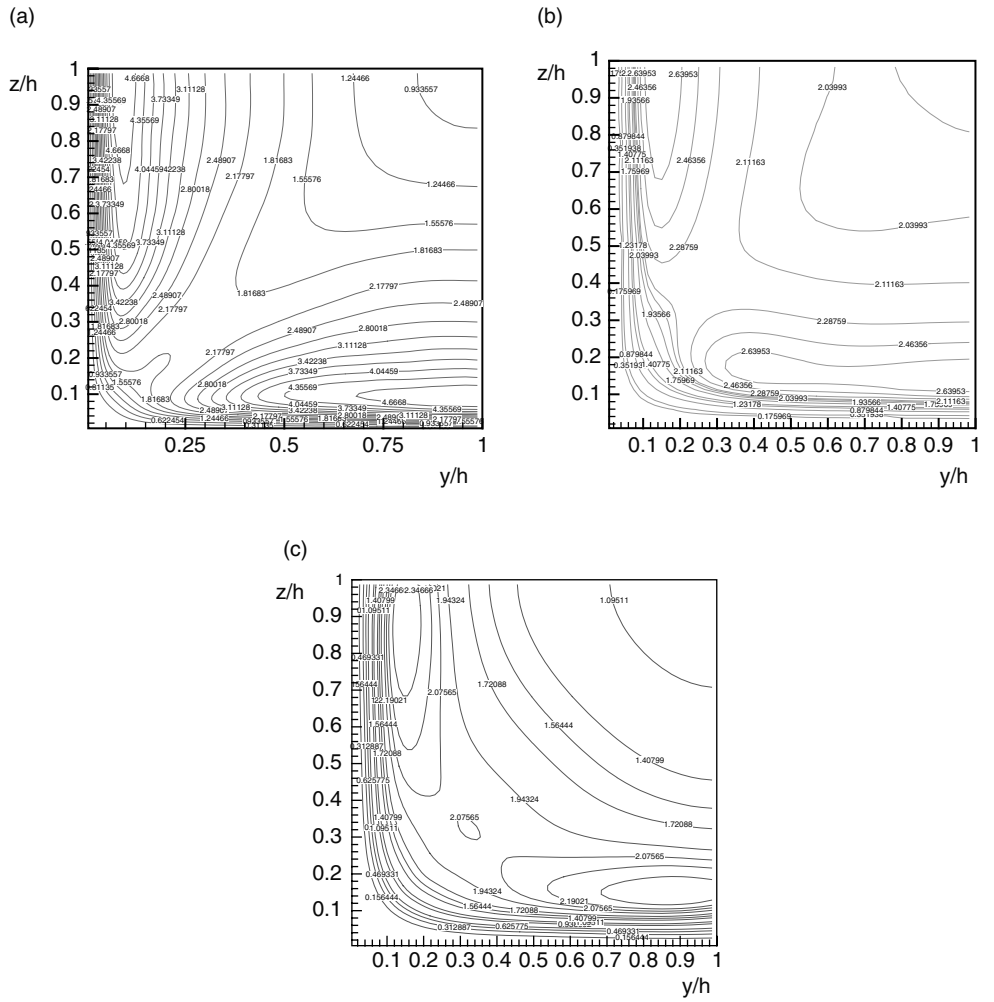

Figure 16 Distribution of the turbulence emergy kinetic k. Comparison of the predictions of the $k-\varepsilon$ and $k-\varepsilon-f\mu$ models with DNS: (a)DNS, (b) $k-\varepsilon-f\mu$, (c)$k-\varepsilon$.

REFERENCES

1. Pope S.B., A more general effective-viscosity hypothesis, *J. Fluid Mech.*, 1975, 72, 331–340.
2. Speziale C.S., Sarkar S. and Gatski T.B., Modelling the presses-strain correlation of turbulence: An invariant dynamical systems approach, *J. Fluid Mech*., 1991, 227, 245–272.
3. Joung Y., Choi S.V. and Choi J.II, Direct numerical simulation of turbulent flow in a square duct : Analysis of secondary flows, *Journal of Engineering mechanics*, 2007, 133 (2), 213–221.
4. Xu H., and Pollard A., Large-eddy simulation of turbulent flow in square annular duct, *Physics of Fluids*, 2001, 13(11), 3321–3337.
5. Vasquez M.S. and Métais O., Large-eddy simulation of the turbulent flow through a heated square duct, *J. Fluid Mech.*, 2002, 453, 201–238.
6. Belhoucine L., Deville M., Elazehari A.R. and Bensalah M.O., Explicit algebraic Reynolds stress model of incompressible turbulent flow in rotating square duct, *Computers & Fluids*, 2004, 33, 179–199.

7. Nishino K., Kasagi N., Turbulence statistics measurement in a two-dimensional channel flow using a three-dimensional particle tracking velocimeter, *Seventh Symposium on Turbulent Shear Flows*, Stanford University, August 21–23, 1989.
8. Mompean G., Numerical simulation of a turbulent flow near a right-angled corner using the Speziale non-linear model with RNG $k - \varepsilon$ equations, *Computers & Fluids*, 1998, 27, 847–859.
9. Huser A. Biringen S. and Hatay F.F., Direct numerical simulation of turbulent flow in a square duct: Reynolds stress budgets, *Physics of Fluids*, 1994, 6 (9), 3144–3152.
10. Gavrilakis S., Numerical simulation of turbulent low-Reynolds-Number flow through a straight square duct, *J. Fluid Mech.*, 1992, 244, 101–129.
11. Huser A. and Biringen S., Direct numerical simulation of turbulent flow in a square duct, *J. Fluid Mech*., 1993, 257, 65–95.
12. Yoshizawa A. and Nisizima S.A., A non equilibrium representation of the turbulent viscosity based on a two-scale turbulent theory, *Physics of Fluids A*, 1993, 5:3302–305.
13. Shih T.H., Zhu J. and Lumley J.L., A new Reynolds stress algebraic equation model, *Comput. Methods Appl. Mech. Eng*., 1995, 125, 287–302.
14. Wallin S. and Johansson A.V., An explicit algebraic Reynolds model for incompressible and compressible turbulent flows, *J. Fluid Mech.*, 2000, 403, 89–132.
15. Gatski T.B., Rumsey C.L., Linear and non-linear eddy viscosity models, Closure Strategies for Turbulent and transitional flows, Launder B.E. and Sandham N.D. eds., *Cambridge University Press*, 2001, 9–46.
16. Yang X.D., Ma H.Y. and Huang Y.N., Prediction of homogeneous flow and a backward facing step slow with some linear and non-linear $k - \varepsilon$ turbulence models., *Nonlinear Science and Numerical simulation*, 2005, 10, 315–328.
17. Speziale C.G. and Abid R., Near wall integration of Reynolds stress turbulence closures with no wall damping, *AIAA Journal*, 1995, 33 (10), 1947–7.
18. Nisizima S., Numerical study of turbulent square-duct flow using an anisotropic $k - \varepsilon$ model, Theo. *Comput. of Fluid Dynamics*, 1990, 2, 183.
19. Patel C.V., Rodi W. and Scheuerer G., Turbulence models for near-wall and low Reynolds number flow: a review, *AIAA Journal*, 1984, 23, 1308–1319.
20. El Yahyaoui O., Mompean G. and Naji H., Evaluation a priori d'un modèle non-linéaire de turbulence, *C.R. Mécanique*, 2002, 330, 27–34, Paris.
21. Naji H., Mompean G. and El Yahyaoui O., Evaluation of explicit algebraic stress models using direct numerical simulations, *Journal of Turbulence* 5, 2004, 38.
22. Leonard B.P., A stable accurate convective modelling procedure based on quadratic upstream interpolation, *Computer Methods in Applied Mechanics and Engineering*, 1979, 19, 59–88.
23. Mompean G., Gavrilakis S., Machiels L. and Deville M.O., On predicting the turbulence-induced secondary flows using non-linear $k - \varepsilon$ models, *Physics of Fluids*, 1996, 8, 1856–1868.
24. Harlow F.H. and Welch J.E., Numerical calculation of time-dependent viscous incompressible flow or fluid with free surface, *Physics of Fluids*, 1965, 8, 2182–2189.
25. Wilcox D.C., Turbulence modelling for CFD. *DCW Indsutries, Inc., 2nd edition*, La cañada, California, 2004.
26. Gavrilakis S., Conditional sampling of the turbulent vorticity field near a smooth corner, *Physics of Fluids*., 1998, 10 (6), 1537–1539.
27. Cheesewright R., McGrath G., and Petty D.G., LDA measurements of turbulent flow in a duct of square cross section at low Reynolds number, Aeronautical Engineering Department, University of London, *Report No. ER 101*, 1990.